

\*Work supported in part by the National Science Foundation, Grant No. GP-16565, and in part by the U. S. Atomic Energy Commission.

- <sup>1</sup>R. J. Adler, B. T. Chertok, and H. C. Miller, *Phys. Rev. C* **2**, 69 (1970); *ibid.* **3**, 2498(E) (1971).  
<sup>2</sup>R. J. Adler, *Phys. Rev. C* **5**, 615 (1972).  
<sup>3</sup>H. P. Noyes, *Nucl. Phys.* **74**, 508 (1965).  
<sup>4</sup>N. Austern and E. Rost, *Phys. Rev.* **117**, 1506 (1960).  
<sup>5</sup>A. Cox, S. Wynchank, and C. Collie, *Nucl. Phys.* **74**, 481 (1965).  
<sup>6</sup>G. Breit and M. L. Rustgi, to be published. This contains a discussion of the capture of polarized  $n$  on polarized  $p$  and the role of the  $^3S$  state in singly radiative capture.  
<sup>7</sup>L. D. Landau, *Nucl. Phys.* **13**, 181 (1959).  
<sup>8</sup>R. E. Cutkosky, *J. Math. Phys.* **1**, 429 (1960).  
<sup>9</sup>J. D. Bjorken, Ph.D. thesis, Stanford University, 1959 (unpublished).  
<sup>10</sup>J. D. Bjorken and S. D. Drell, *Relativistic Quantum Fields* (McGraw-Hill, New York, 1965), p. 235.  
<sup>11</sup>M. Gell-Mann and M. Goldberger, *Phys. Rev.* **96**, 1433 (1954).  
<sup>12</sup>F. Low, *Phys. Rev.* **96**, 1428 (1954).  
<sup>13</sup>G. F. Chew, *S-Matrix Theory of Strong Interactions* (Benjamin, New York, 1961), p. 30.

- <sup>14</sup>F. Gross, *Phys. Rev.* **140**, B410 (1965).  
<sup>15</sup>R. J. Adler, Ph.D. thesis, Stanford University, 1965 (unpublished), p. 106.  
<sup>16</sup>F. Kaschluhn and K. Lewin, *Nucl. Phys.* **87**, 73 (1966). An error in this paper is discussed in Ref. 1.  
<sup>17</sup>R. J. Adler, *Phys. Rev.* **141**, 1499 (1966).  
<sup>18</sup>R. J. Adler, *Phys. Rev.* **169**, 1192 (1968); **174**, 2169(E) (1968).  
<sup>19</sup>E. J. Squires, in *4th Scottish Universities Summer School*, edited by R. G. Moorehouse (Plenum, New York, 1965).  
<sup>20</sup>L. I. Lapidus and Chou Kuang-Chao, *Z. Eksperim. i Teor. Fiz.* **39**, 1286 (1960) [transl.: *Soviet Phys. - JETP* **12**, 898 (1961)].  
<sup>21</sup>I. J. Kalet, *Phys. Rev.* **176**, 2135 (1968).  
<sup>22</sup>N. K. Glendenning and G. Kramer, *Phys. Rev.* **126**, 159 (1962).  
<sup>23</sup>J. M. Blatt and V. F. Weisskopf, *Theoretical Nuclear Physics* (Wiley, New York, 1952), p. 63.  
<sup>24</sup>B. Sakita and C. Goebel, *Phys. Rev.* **127**, 1787 (1962).  
<sup>25</sup>M. Skolnick, *Phys. Rev.* **136**, B1493 (1964).  
<sup>26</sup>B. Bosco, C. Ciocchetti, and A. Molinari, *Nuovo Cimento* **28**, 1427 (1963).  
<sup>27</sup>G. Stranahan, *Phys. Rev.* **135**, B953 (1969).

## Regge Description of Optical-Model Scattering

T. Tamura and H. H. Wolter\*

*Center for Nuclear Studies, University of Texas,† Austin, Texas 78712*

(Received 28 August 1972)

The analytic continuation of the  $S$  matrix into the complex angular momentum plane is performed exactly for the Woods-Saxon-type optical potentials, describing the elastic scattering of spinless but charged particles. The properties of this  $S$  matrix, such as the nature of the pole trajectories and the behavior of the background integral, are investigated for several specific cases. Based on these exact calculations, the validity of various approximations made in the Regge theory is assessed. It is found that approximations which retain only the pole terms are generally poor, being quite sensitive to the number and the positions of the poles and converging very slowly with an increasing number of poles. On the other hand, models using a simple analytic background term, in addition to one pole term, are found to reproduce the exact Regge amplitude quite accurately under favorable conditions. Suggestions are made for the possibility of extending this idea into a background-plus-several-pole model, when the background-one-pole model fails.

### I. INTRODUCTION

Since the complex angular momentum approach was first introduced by Regge *et al.*,<sup>1</sup> it has been applied mostly to the relativistic rather than the nonrelativistic domain, in spite of the fact that various mathematical manipulations basic to the approach can be made rigorously only in the latter domain. The reason for this could have been that in nuclear and atomic physics, very little seems to be gained from this approach beyond what can

be obtained by more conventional methods. However, interest has been revived recently, perhaps in relation to an increased investigation of heavy-ion-induced nuclear reactions. One finds that the scattering of such strongly absorbed particles can be described more easily and more uniquely in terms of a smooth cutoff  $S$  matrix, in contrast to optical-model fits which suffer from many discrete and continuous ambiguities.<sup>2</sup> More recently it was shown that the strong backward rise seen in heavy-ion scattering cross sections

can rather well be reproduced by the addition of a single-pole term to such a smooth cutoff term.<sup>3,4</sup> Such a pole may very well be interpreted as a Regge pole. Other regions, where Regge theory is potentially of great interest, are processes in which a large number of smoothly varying  $S$  matrix elements contribute, as e.g., in Coulomb excitation. The scattering amplitude there can sometimes be expressed in terms of a few Regge poles. This approach has already been applied in the description of atom-atom scattering.<sup>5</sup>

In the Regge theory<sup>1</sup> the scattering amplitude is represented as a sum of pole terms plus a background integral, usually taken along the imaginary axis. It is the background integral about which least is known in practical applications. One approach followed mainly by Mukherjee and Shastri,<sup>6,7</sup> has been to modify the pole term in a suitable way, so that one is justified in neglecting the background term completely. These pole approximations of increasing complexity have been used to describe various cross sections.<sup>8,9</sup> In another approach, which we already mentioned, the background term is retained, being parametrized in a simple analytical form and one or more pole terms, also parametrized, are added. With such a form, successful fits have been achieved to  $\alpha$  and  $^{16}\text{O}$  scattering.<sup>3,4</sup>

In order to establish the validity of such approximate or phenomenological approaches, however, it is desirable to know the exact behavior of pole and background terms. Unfortunately, detailed knowledge of the analytic continuation of the  $S$  matrix into the complex angular momentum plane has been all but restricted to Hamiltonians with a superposition of Yukawa potentials,<sup>10</sup> and essentially nothing is known for the case of the Woods-Saxon potentials, which are conventionally used in nuclear physics. We therefore felt it worthwhile to investigate exactly (i.e., numerically) the analytic continuation of the  $S$  matrix for such an optical potential and to study the exact behavior of the pole and background terms. To present the results of such an investigation is the purpose of this present paper.

In Sec. II we briefly review Regge theory, as we need it to explain our calculations that follow. In Sec. III we discuss some of the problems encountered in the actual numerical calculations of the  $S$  matrix for arbitrary values of the complex angular momentum. In Sec. IV we apply the theory to the elastic scattering of neutrons by nuclei at low energies and investigate the validity of the pole approximations of Mukherjee and Shastri.<sup>8</sup> We then go on in Sec. V to study the elastic scattering between heavy ions, taking as an example the case of  $^{16}\text{O}$  on  $^{16}\text{O}$ . McVoy<sup>4</sup> has already done a rather

detailed analysis of this case with a parametrization of the  $S$  matrix. We complement his considerations in Sec. VI by comparing his results with exact Regge representations. A brief summary and conclusion are given in Sec. VII. A preliminary account of this work has already been reported on two earlier occasions.<sup>11</sup>

## II. BRIEF REVIEW OF REGGE THEORY

The amplitude for the scattering between two spinless particles is normally given as

$$A(k, \theta) = A_C(\theta) + \frac{1}{2ik} \sum_l (2l+1) e^{2i\sigma_l} (S_l - 1) P_l(\cos\theta), \quad (1)$$

with the Rutherford amplitude

$$A_C(\theta) = -\frac{\eta}{2k \sin^2 \frac{1}{2}\theta} \exp(-i\eta \ln \sin^2 \frac{1}{2}\theta + 2i\sigma_0). \quad (2)$$

Let us further define for future convenience a nuclear amplitude

$$A_N(\theta) = \frac{1}{2ik} \sum_l (2l+1) (S_l - 1) P_l(\cos\theta). \quad (3)$$

The  $S$  matrix can be continued analytically into the right half of the complex  $\lambda$  plane ( $\lambda = l + \frac{1}{2}$ ), and the sum in (3) may be converted into an integral over a contour  $C$  in the right half plane enclosing the real  $\lambda$  axis:

$$A_N(\theta) = -\frac{\pi i}{k} \sum_n \lambda_n \beta_n P_{\lambda_n - 1/2}(-\cos\theta) / \cos(\pi\lambda_n) + \frac{1}{2k} \int_C d\lambda \lambda [S(\lambda) - 1] P_{\lambda - 1/2}(-\cos\theta) / \cos(\pi\lambda), \quad (4)$$

where  $\lambda_n$  are the poles of  $S(\lambda)$  enclosed by the contour  $C$  with residues  $\beta_n$ . If further the continuation has the property

$$|S(\lambda) - 1| \sim O(1/|\lambda|) \quad \text{for } |\lambda| \rightarrow \infty, \quad \text{Re}\lambda \geq 0, \quad (5)$$

then the contour can be deformed to run along the imaginary axis, and we get the Sommerfeld-Watson transform of the nuclear amplitude.<sup>10</sup>

The representation (4) can be generalized. One may perform a partial-wave projection on Eq. (4) to obtain

$$S_l - 1 = \sum_n \frac{2\lambda_n}{\lambda^2 - \lambda_n^2} \beta_n + \frac{1}{2\pi i} \int_C d\lambda' \frac{2\lambda' [S(\lambda') - 1]}{\lambda^2 - \lambda'^2} \quad (6)$$

and use this expression in evaluating the sum in

(1). In general one can always use Cauchy's theorem to represent the function  $[S(\lambda) - 1]$ , which is meromorphic in the right half plane, in the form<sup>6</sup>

$$S_i - 1 = \sum_n \frac{\beta_n F(\lambda, \lambda_n)}{\lambda - \lambda_n} + \frac{1}{2\pi i} \int_C d\lambda' \frac{[S(\lambda') - 1] F(\lambda, \lambda')}{\lambda - \lambda'}, \quad (7)$$

where  $F(\lambda, \lambda')$  is an arbitrary analytic function, which is regular and bounded for  $\text{Re}\lambda \geq 0$  and  $\text{Re}\lambda' \geq 0$  and satisfies  $F(\lambda, \lambda) = 1$ . We can even allow  $F$  to have isolated singularities in the right half plane and also to violate the requirement that  $F(\lambda, \lambda) = 1$ . Then we have the representation

$$(S_i - 1)F(\lambda, \lambda) = \sum_n \frac{\beta_n F(\lambda, \lambda_n)}{\lambda - \lambda_n} + \sum_k \frac{\gamma_k [S(\lambda_k) - 1]}{\lambda - \lambda_k} + \frac{1}{2\pi i} \int_C d\lambda' \frac{(S - 1)F(\lambda, \lambda')}{\lambda - \lambda'}. \quad (8)$$

Here the second sum runs over the poles  $\lambda_k$  of  $F(\lambda, \lambda')$  enclosed by the contour  $C$  for a fixed  $\lambda$ , and  $\gamma_k$  are the corresponding residues. If the particular choice

$$F(\lambda, \lambda') = 2\lambda' / (\lambda + \lambda') \quad (9)$$

is made, Eq. (7) is reduced to Eq. (6), the original Regge representation. In the following the terminology "Regge representation" is used in this restricted sense only. In case we make other choices of  $F(\lambda, \lambda')$ , we call them "modified Regge representations."

The property (5), which is essential for the possibility of performing the Sommerfeld-Watson transformation, has been proved only for the case of superpositions of Yukawa potentials.<sup>1</sup> In applying the Regge techniques to nuclear physics one encounters Woods-Saxon potentials with complex strengths. It is known that even with the (absorptive) imaginary potential the fourth quadrant is still free from poles,<sup>8</sup> but as we shall see later, the behavior of the trajectories and of the background term is otherwise quite different from that of the Yukawa potential.

The general unitarity relation for the  $S$  matrix of a complex potential  $U$  reads

$$S(\lambda, k, U) = S^*(\lambda^*, k^*, U^*)^{-1}. \quad (10)$$

Thus with each pole there is associated a zero of the  $S$  matrix. For real potential and positive energy these lie symmetrically with respect to the real axis. For complex potentials we shall see, that both the pole and the zero are shifted upwards.

Even though all moments of a Woods-Saxon potential are finite, the property (5) does not follow.

One can only show in general that<sup>10</sup>

$$|S(\lambda)| \rightarrow \begin{cases} 0, & \text{Im}\lambda \rightarrow \infty \\ \infty, & \text{Im}\lambda \rightarrow -\infty, \end{cases} \quad (11)$$

and this is verified in actual numerical calculations. It can nevertheless be shown that, for any potential with finite range,

$$|S(\lambda) - 1| \sim e^{-\xi\lambda}, \quad \text{Re}\lambda \rightarrow \infty (\xi > 0). \quad (12)$$

Thus in general the scattering amplitude can be represented by pole and background terms, but the background integral cannot be made to run along the imaginary axis; it must eventually be bent so that  $\text{Re}(\lambda) \rightarrow \infty$ . While this prevents the application of the Regge theory in high energy physics, since it changes the asymptotic behavior in  $z = \cos\theta$ , it does not necessarily impair its application in low energy physics, where to choose the background path along the imaginary axis has no specific significance. In low energy physics the modified Regge representations may in general be regarded as a method to separate the dominant pole contributions from a smooth background term.

As mentioned in the Introduction, application of Regge theory in nuclear physics has been done essentially in two ways. One approach<sup>6-9</sup> attempts to represent the scattering amplitude only in terms of a few poles of the  $S$  matrix. This meets a serious difficulty if the Regge representation (9) is used. The  $S$  matrix (7) for the sum of a finite number of poles decreases with  $\lambda$  only as  $\lambda^{-2}$  and not exponentially as required in (12). The exponential decrease in this representation is only achieved by considering infinitely many poles, including those in the left half plane. Therefore, if only a finite number of poles is to be considered, the freedom in the choice of the functions  $F(\lambda, \lambda')$  has to be employed to achieve the correct asymptotic behavior in  $\lambda$  and the threshold behavior in  $k$  of the  $S$  matrix element (7), and at the same time the smallness of the background term. One such function, which was used to describe the scattering of uncharged particles,<sup>9</sup> is

$$F(\lambda, \lambda') = \frac{\exp(i e^{-\lambda\xi}) - 1}{\exp(i e^{-\lambda'\xi}) - 1} \frac{e^{-R/a} + e^{-\lambda'\xi}}{e^{-R/a} + e^{-\lambda\xi}} \times \exp\left(i\theta \frac{\lambda' - \lambda}{\lambda' + \lambda}\right) \left(\frac{\lambda'}{\lambda} \frac{2\lambda'}{\lambda + \lambda'}\right), \quad (13)$$

where  $R$  and  $a$  are the radius and diffuseness of the potential used, and

$$\xi = \cosh^{-1}(1 + \mu^2/2k^2),$$

$\mu$  and  $\theta$  being additional parameters. We shall compare our exact results with this specific approximation later. The representation (13) will

be called the " $P_3$  representation," as it was done in Ref. 9.

In the other approach one keeps only the most important Regge pole and parametrizes it, as well as the background term.<sup>3,4</sup> In the scattering of strongly absorbed particles, the average behavior of the  $S$  matrix can be described well by a smooth cutoff model<sup>12</sup>:

$$S_l = \{1 + \exp[-i\alpha + (L - l)/\Delta]\}^{-1} \equiv B(l). \quad (14)$$

Yet individual partial wave can deviate strongly from this form and this deviation may be described by introducing a Regge pole. Thus McVoy<sup>4</sup> used the following parametrization:

$$S_l = B(l) \frac{l - L_0 - iz(l)}{l - L_0 - ip(l)} = B(l) \left[ 1 + i \frac{D(l)}{l - L_0 - \frac{1}{2}i\Gamma(l)} \right], \quad (15)$$

where  $p = \frac{1}{2}\Gamma$  and  $z = \frac{1}{2}\Gamma - D$ . The first form shows explicitly the appearance of a zero associated with a pole according to Eq. (10), while the second form represents the  $S$  matrix as a background term plus a pole term with residue function equal to  $B$  times  $D$ . The function  $D(l)$  of the pole term was chosen<sup>4</sup> to be exponentially decreasing in  $l$  in order to satisfy (12):

$$D(l) = D(1 + e^{(l-L)/\Delta})^{-1}, \quad (16)$$

and  $\Gamma(l)$  was chosen to have the same  $l$  dependence for no obvious reason.

In this parametrization the pole term decreases exponentially in  $l$  on both sides of the pole  $L_0$ , while in the Regge representation (9) it decreases only as  $l^{-2}$ , as we have remarked above. With the purpose of comparing later in Sec. VI the exact amplitude with this parametrization, it is desirable to introduce a representation which also has exponential behavior. We thus propose the representation

$$F(\lambda, \lambda') = 2 / \{1 + \cosh[(\lambda - \lambda')/\Delta]\}, \quad (17)$$

which shall henceforth be called the  $\Delta$  representation. It localizes the contribution of a Regge pole to a range in angular momentum determined by the parameter  $\Delta$ , facilitates the summation of the partial wave sum in (1), since the pole terms now decrease exponentially in  $l$ , and also damps out the background integral quickly in a direction parallel to the real axis. This function has poles at the positions

$$\lambda_k = \lambda + i\pi\Delta(2k+1), \quad k \text{ integer}. \quad (18)$$

Since these are poles of order 2 they do not contribute to the  $S$ -matrix representation (8). Nevertheless, care should be exercised so that these poles are not too close to any of the Regge poles

which are taken into account explicitly, because then the contribution of that pole would be enhanced artificially. This will in practice present no problem, however, because this representation has been constructed so as to isolate the contributions of poles in the vicinity of the real axis. Since  $\Delta$  is usually taken to be greater than about 1.5, the poles (18) of  $F$  are removed sufficiently far from the real axis.

### III. REMARKS ON NUMERICAL CALCULATIONS

In order to calculate an  $S$  matrix element in any representation one has to be able to calculate the analytic continuation  $S(\lambda)$  for any value of  $\lambda$  in the right half complex  $\lambda$  plane. We want to do this for an optical-model potential of the Woods-Saxon shape, excluding in this work a spin-orbit term. The numerical procedure is very similar to the one used in standard optical-model calculations. However, there are a few complications which might be worth discussing briefly.

One has to find the regular solution of the Schrödinger equation,

$$\left( \frac{\hbar^2}{2m} \frac{d^2}{dr^2} + E - V(r) - \frac{\hbar^2}{2m} \frac{\lambda^2 - \frac{1}{4}}{r^2} \right) \psi(\lambda, k, r) = 0, \quad (19)$$

which at the origin behaves as

$$\psi(\lambda, k, r) \sim r^{\lambda+1/2} = r^{\alpha+1/2} e^{i\beta \ln r}, \quad r \rightarrow 0, \quad (20)$$

with  $\lambda = \alpha + i\beta$ . Although the magnitude of  $\psi$  decreases to zero at the origin, the phase oscillates increasingly rapidly. It is therefore necessary to start the numerical integration at some distance away from the origin. To supply the starting values of the regular solution at a finite radius the potential and the wave function are expanded in power series around the origin, in a way similar to that used by Burke and Tate.<sup>13</sup>

The  $S$  matrix is obtained as<sup>10</sup>

$$S(\lambda, k) = \frac{F_+(\lambda, k)}{F_-(\lambda, k)} = \frac{W(\psi, f_+)}{W(\psi, f_-)}, \quad (21)$$

where  $W(f, g) = f'g - g'f$  is the Wronskian of  $f$  and  $g$ . The  $F_{\pm}$  are generalized Jost functions, and  $f_{\pm}$  are the irregular solutions of (16) with  $V=0$ , which behave asymptotically as

$$f_{\pm}(\lambda, k, r) \sim \exp[\mp i(kr - \frac{1}{2}\lambda\pi)]. \quad (22)$$

If a Coulomb interaction is present these are Coulomb functions of complex order, which can be calculated in very much the same way as for complex energy.<sup>14</sup> Irrespective of the presence or absence of the Coulomb interaction, it should be

noted that the behavior of  $f_{\pm}$  for  $\text{Im}\lambda = \beta - \infty$  is given by

$$f_{\pm}(\lambda, k, r) \sim e^{\mp\pi\beta/2}, \quad \beta \rightarrow \infty, \quad (23)$$

while  $\psi$  also increases as  $e^{\pi\beta/2}$ . Therefore the two terms in the Wronskian  $F_-$  are  $O(e^{\pi\beta})$ , while those in  $F_+$  are  $O(1)$ . Since  $S$  is known to be  $O(1)$ , if the potential is not too strong, the above argument shows that two large terms cancel very strongly with each other in  $F_-$ . Thus a very careful and precise numerical calculation is needed to get accurate  $S$  matrix elements along the imaginary axis.

Regge poles can be located by finding the zeros of  $F_-(\lambda)$  by Newton's method. The corresponding residues are then given by

$$\beta_n = F_+(\lambda_n) \left/ \left[ \frac{d}{d\lambda} F_-(\lambda) \right]_{\lambda=\lambda_n} \right. . \quad (24)$$

Similarly, one may find the zeros of  $S(\lambda)$  by looking for the zeros of  $F_+(\lambda)$ . There is always a simple way to confirm whether one has located all the poles within a given contour, if one knows the values of  $S(\lambda)$  along this contour. The relation

$$\frac{1}{2\pi i} \int_C d\lambda' S(\lambda') = \sum_n \beta_n \quad (25)$$

must be satisfied always.

In the present work we always calculate cross sections from Eq. (1), where  $(S_l - 1)$  is obtained from Eq. (7). Often we shall refer to cross sections obtained from the background term only and/or from the pole term only. By the former we mean that we take only the background term of Eq. (7) and insert it into Eq. (1), while for the latter we take only the pole term of (7) in (1) and, moreover, suppress the Coulomb amplitude  $A_C(\theta)$  there; we do not want to include  $A_C(\theta)$  twice. We combine the Coulomb amplitude with the background amplitude, because in all the cases considered here involving charged particles the two almost cancel each other, making the sum of the two comparable to the pole amplitude. The pole amplitude is usually much smaller than the other two considered separately.

For clarity of presentation in the following sections we shall introduce a shorthand notation, to denote the way in which a certain  $S$  matrix element or a cross section was calculated. We use the superscript  $(r, t, p)$  where, first,  $r$  denotes the representation, with  $R$  meaning Regge representation (9),  $\Delta$  the  $\Delta$  representation (17), and  $P_3$  the  $P_3$  representation (13); also  $E$  will stand for the exact optical-model results. Secondly,  $t$  denotes the term, with  $B$  meaning background term,  $P$  meaning pole term, and  $T$  meaning total, i.e., the sum of the two. Finally, we shall let  $p$  specify the poles which are included explicitly in the

pole term. Note that the background term also depends on  $p$ , because the integration path depends on  $p$ . The poles are named by the main quantum number  $n$ , unless other types of poles are considered. As an example  $d\sigma^{(R,P,n=0)}$  is the differential cross section calculated from the pole term of the Regge representation (9) with the  $n=0$  pole only. When there is no danger of confusion, any of these symbols may be absent. E.g.,  $|S_l^{(B)}|$  means the absolute value of the  $S$  matrix calculated from the background term, where no definite representation and poles have been specified, or are obvious from the context.

#### IV. APPLICATION TO THE SCATTERING OF NEUTRONS BY NUCLEI

We first study the elastic scattering of neutrons to assess the validity of various pole approximations.<sup>8</sup> This will also give us our first insight into the analytic properties of the  $S$  matrix of the Woods-Saxon potential. The following potential parameters were fixed by Campbell *et al.*<sup>15</sup> to fit the over-all behavior of the scattering of 1- to 5-MeV neutrons by a variety of nuclei;

$$U(r) = -(V + iW)(1 + e^{(r-R)/a})^{-1},$$

where

$$V = 52 \text{ MeV}, \quad W = 3.12 \text{ MeV}, \quad (26)$$

$$R = 1.15A^{1/3} + 0.4 \text{ fm}, \quad a = 0.52 \text{ fm}.$$

The pole trajectories with this potential for  $E_{\text{lab}}$  ranging from 0 to 10 MeV when  $A = 40$  are shown in Fig. 1. Here the imaginary potential has been decreased linearly below 1 MeV, so that it becomes zero at  $E_{\text{lab}} = 0$ . The  $n=0$  and  $n=1$  trajectories are seen to leave the real axis after, respectively, passing through  $l=3$  and  $l=1$ , and their corresponding bound states were located. The  $n=0$  trajectory leaves the real axis with an extremely small angle and, for low positive energies, has very small residues. The  $n=2$  trajectory leaves the real axis before it reaches  $l=0$ , and therefore leaves in the backward direction<sup>10</sup>; it also does not give rise to a bound state. In Fig. 1 there is also shown a zero-type trajectory,<sup>10</sup> which at  $E_{\text{lab}} = 0$  emerges from  $\lambda = 0$  and for low positive energies moves very rapidly with energy. Other trajectories of this type may also exist, but no extensive search was made.

The background integral was calculated for  $E_{\text{lab}} = 2.5$  MeV along two paths,  $C_1$  and  $C_2$ , indicated in Fig. 1. With the residue theorem (25) it was confirmed that there are no more poles enclosed by contour  $C_1$ , but that further poles exist enclosed by the contour  $C_2$ , some of which may be other zero-type poles. The calculations verified that

along the imaginary axis the S matrix indeed behaves as was predicted by Eq. (11).

In Fig. 2 the differential cross section at  $E_{\text{lab}} = 2.5$  MeV is given in various representations. The accuracy of our calculations was checked by verifying that the cross section  $d\sigma^{(R,T)}$  equals the exact cross section  $d\sigma^{(E)}$ , calculated directly from the physical  $\lambda$ , i.e., obtained with the conventional optical-model calculations. Other cross sections shown in Fig. 2 are  $d\sigma^{(R,B, n=0-2)}$  calculated with the background term only taken along contour  $C_1$ , and  $d\sigma^{(R,P, n=0-2)}$ , calculated with the poles  $n = 0, 1$ , and  $2$  enclosed by  $C_1$ . As is seen the background contributes most strongly at small angles, while the pole term dominates at large angles, the  $n=0$  pole contributing most strongly among the others. Both background and pole terms diverge at  $0^\circ$ , since they do not have separately the correct asymptotic behavior in  $\lambda$  in the Regge representation.

The pole approximations were studied for this case in Ref. 8, using expression (13) for  $F(\lambda, \lambda')$ , and the cross section with this  $P_3$  representation are also shown in Fig. 2. (In obtaining, or reproducing, these cross sections we corrected slight numerical inaccuracies which we believe were committed in Ref. 8.) The parameter  $\theta$  in (13) is taken as  $-50^\circ$ . In Ref. 8 the value used for  $\mu$  was not specified, but it must have been close to  $\mu$

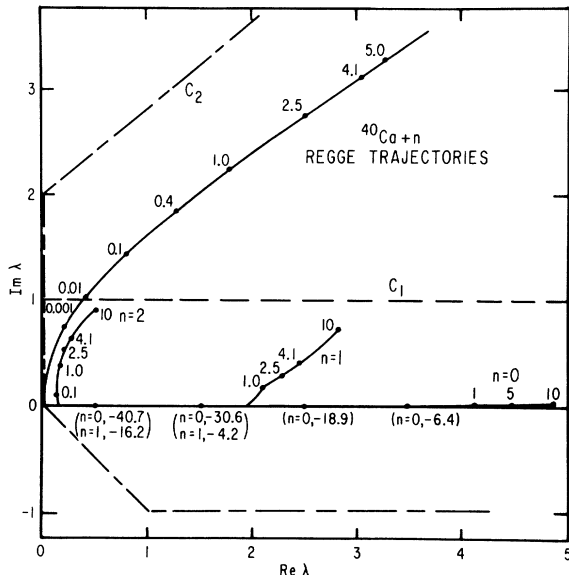


FIG. 1. Regge trajectories for  $^{40}\text{Ca}(n, n)$  obtained by using the potential (26). The  $n=0$  to  $2$  and one zero-type trajectories are shown. The numbers attached to the trajectories give  $E_{\text{lab}}$  in MeV. Bound states are indicated on the real axis together with their binding energies. Two contours  $C_1$  and  $C_2$  are indicated, along which the background integral was evaluated.

$= 1/a$ , which is what we used.

As is seen in Fig. 2, the result with the  $P_3$  representation is much better than that with the Regge representation,<sup>8</sup> if only the contributions from the  $n=1$  and  $n=2$  poles were considered. Note, however, that Ref. 8 failed to locate the  $n=0$  pole, possibly because it is very weak. If this pole is included, as it should, the cross section gets about 1 order of magnitude larger than it was otherwise, and therefore than the exact cross section. This means that the background terms must have also been quite large, so as to cancel the pole term, showing that the  $P_3$  representation failed to decrease the contribution of the background term, contrary to what was expected. Note that the very weak  $n=0$  pole contributes so strongly, because the first factor of  $F(\lambda, \lambda')$  of (13) increases exponentially with increased  $\text{Re}(\lambda')$ . For this very same reason the direct calculation of the background term is rather difficult, because the integrand diverges with  $\text{Re}(\lambda') \rightarrow \infty$ , as well as with  $\text{Im}(\lambda') \rightarrow \infty$ , as is seen from Eq. (11).

We feel that it is extremely difficult to find a representation in which one can replace with high accuracy the background term by a sum of pole terms. One may succeed to do so only under certain very fortunate circumstances, if any.

#### V. APPLICATION TO THE SCATTERING OF $^{16}\text{O}$ BY $^{16}\text{O}$

We now turn to the scattering of strongly absorbed particles, where Regge theory has been applied most successfully.<sup>3,4</sup> One such effect was observed in the elastic scattering of  $^{16}\text{O}$  on  $^{16}\text{O}$ , where the excitation function at  $90^\circ$  exhibits broad prominent peaks at energies between 20 and 30 MeV in the c.m. system.<sup>16</sup> This excitation function could be fitted qualitatively with a very shallow optical-model potential,

$$V = 17 \text{ MeV}, \quad W = 0.1 E_{\text{c.m.}}, \quad (27)$$

$$R = 6.8 \text{ fm}, \quad a = 0.49 \text{ fm},$$

but this fit does not reproduce the peak-to-valley ratio of the peaks observed in the experiment. Chatwin *et al.*<sup>17</sup> later improved the situation by making the imaginary potential angular-momentum-dependent

$$V = 16 \text{ MeV}, \quad W = (0.5 E_{\text{c.m.}} - 7) \left( 1 + \exp \frac{l - l_c}{\Delta l} \right)^{-1} \text{ MeV}. \quad (28)$$

This extension of the optical model may be justified by considering the decrease of the possible number of open channels<sup>17</sup> or the density of levels in the compound system<sup>18</sup> with increasing angular momentum. The cutoff angular momentum  $l_c$  in-

creases slowly with energy, while  $\Delta l$  is fixed at 0.4.

When continuing into the complex plane the  $S$  matrix associated with the potential (28), it should be noted that the cutoff factor has infinitely many poles in the complex plane located at

$$p_j = l_c + i\pi\Delta l(2j + 1) \quad (j = \text{integer}), \quad (29)$$

and thus lying on a straight line perpendicular to the real axis at  $l_c$ . The distance of the nearest poles from the real axis is  $\pi\Delta l \approx 1.2$ . These poles introduce singularities into the  $S$  matrix. We have not established the precise nature of these singularities of  $S$  at  $p_j$ , but they are believed to be essential. We found a large number of poles of  $S(\lambda)$  in the vicinity of each  $p_j$ . As a function of energy these seem to emerge from  $p_j$ , and then move away from it slowly with increased energy. In order to calculate the contribution of all these unknown singularities, we draw a small closed loop around each  $p_j$ , and carried out a contour integral along this loop. As is seen in Table I, given below, their contributions are rather small in gen-

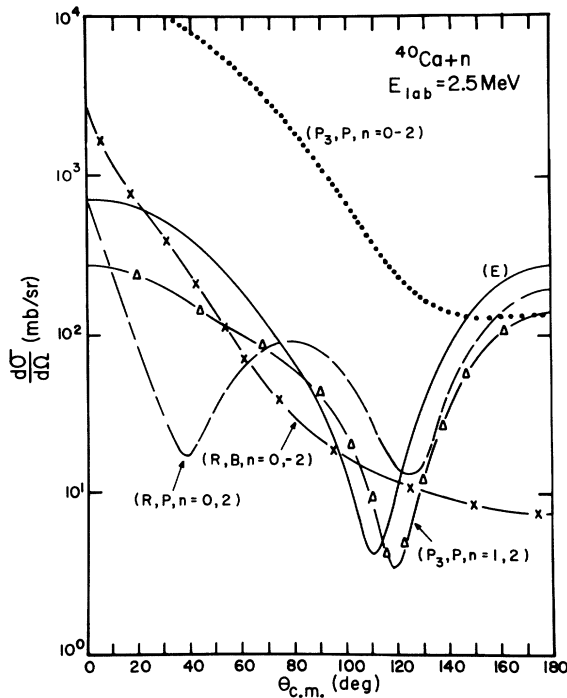


FIG. 2. Differential cross sections for  $^{40}\text{Ca}(n, n)$  at  $E_{\text{lab}} = 2.5$  MeV. The notation used to label the curves here and in most of the other figures was described at the end of Sec. III. Thus (E) is the exact result, while (R, P,  $n = 0 - 2$ ) and (R, B,  $n = 0 - 2$ ), respectively, are the cross sections calculated in the Regge representation with the  $n = 0 - 2$  pole terms and the background term only. Also given here are pole approximations in the  $P_3$  representation (13) of Ref. 8.

eral compared with the poles of single-particle-resonance character.

Figure 3 shows the Regge trajectories calculated for the potential (28). As is seen they can be classified into two types. The first type of trajectory is that just discussed, i.e., that associated with the singularities of the angular momentum cutoff factor in the potential. We show only a few of them. Note that these poles also appear in the fourth quadrant, even though it is known that there should be no poles for a potential without spin-orbit interaction as long as the imaginary part is negative. The angular-momentum-dependent imaginary potential, however, can be positive effectively in the vicinity of the singularity, and this is the reason the poles appear in the fourth quadrant.

The second type of trajectory is of single-particle-resonance (SPR) character, and is labeled in Fig. 3 with the corresponding radial quantum number  $n$ , which ranges from 0 through 5. (The classification of the trajectory  $n = 5$  as a SPR trajectory is of course quite academic, since it never comes close to the real axis at all.) Such SPR trajectories also exist for Yukawa potentials and for them their behavior is well known.<sup>10</sup> They emerge from the real axis at zero energy, moving first to the right and eventually turn up and move back into the left half plane.

As is seen in Fig. 3 the behavior of the SPR trajectories for the Woods-Saxon potential is quite different from this. As is exemplified by the  $n = 4$  and 5 trajectories, they can enter the first quadrant across the imaginary axis at  $\text{Im}(\lambda) \neq 0$ . Except for  $n = 0$  the SPR trajectories are almost straight moving into the upper right corner. The  $n = 0$  trajectory begins to be bent at the energy where the real part of the pole approaches  $l_c$ , because then the absorption becomes weaker, and for weaker absorption the trajectories lie usually closer to the real axis, as will be discussed later in relation to Fig. 12. In fact the  $n = 0$  trajectory, calculated for the  $l$ -independent potential (27) and shown in Fig. 4, is also straight, while the other SPR trajectories behave similarly as they did in Fig. 3. In this figure we followed the trajectories to energies of  $E_{\text{c.m.}} = 60$  to 100 MeV (out of curiosity since our model loses its physical significance there). It is seen, that the trajectories continue to be almost straight and to move into the upper right corner. They show no indication of bending back into the left half plane.

The value of  $l$ , the real part of the  $n = 0$  pole position is a unique function of  $E_{\text{c.m.}}$ , and we found that  $E_{\text{c.m.}}$  and  $l(l + 1)$  are proportional to each other to a high accuracy for  $E_{\text{c.m.}} = 15$  to  $\sim 30$  MeV, when the trajectory is calculated for the po-

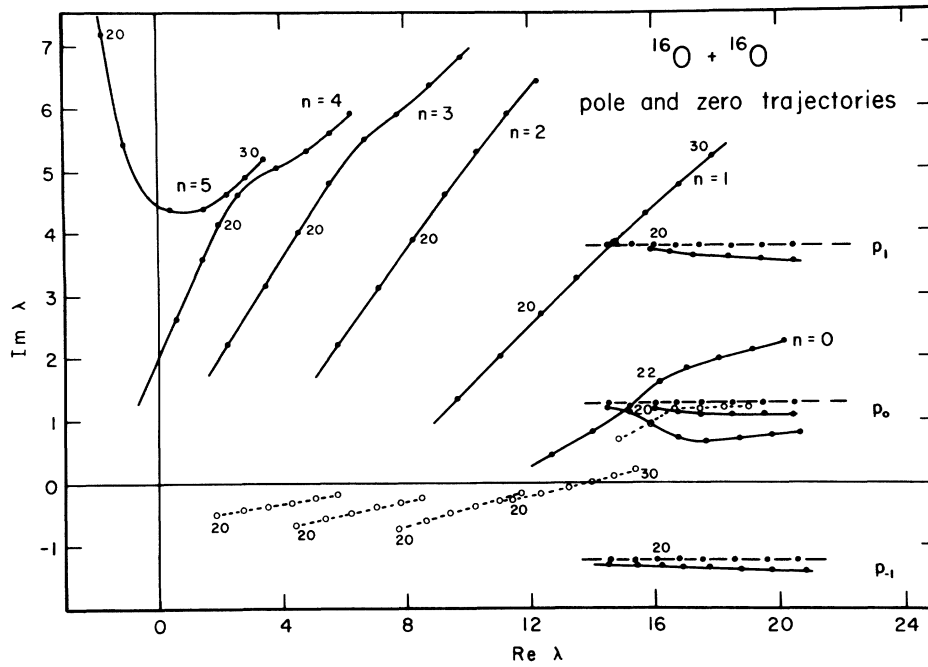


FIG. 3. Trajectories of poles (solid) and zeros (dashed) for the  $^{16}\text{O}$ - $^{16}\text{O}$  elastic scattering with the angular-momentum-dependent potential (28). The singularities of the angular momentum cutoff factor are denoted by  $p_j$ , and some of the poles associated with them are shown. The pole trajectories labeled  $n = 0$  through 5 correspond to single-particle resonances. With each pole there is associated a zero of the  $S$  matrix and some of these are also shown. The numbers attached to the trajectories are  $E_{c.m.}$  in MeV and the points on the curves are given in intervals of 2 MeV.

tential (27) [more specifically we have the relation  $E_{c.m.} \approx 0.056l(l+1) + 6.75$  MeV], a fact which has recently been noted by Arima, Scharff-Goldhaber, and McVoy.<sup>19,20</sup> This result is not unexpected, however, since a partial wave with angular momentum  $l$  will resonate when  $E_{c.m.}$  is such that the

position  $r = l/k$  of the first maximum of this wave equals the radius of the trapping potential, which is located just behind the potential barrier and thus very close to the nuclear radius  $R$ .

This proportionality of  $E_{c.m.}$  to  $l(l+1)$  may motivate one to interpret a resonant state at  $E_{c.m.}$ , corresponding to an integer value of  $l$ , to be a member of a rotational band. In fact, as we noted above, the intrinsic state of these resonances is independent of  $l$ : Two ions, retaining their own identities, are separated from each other by a distance which is approximately independent of  $l$ . One may likewise call these resonances molecular states,<sup>19</sup> but it may simply be a matter of terminology. Probably the most unambiguous understanding is to call them simply a series of single-particle resonances.<sup>21</sup>

Referring back to the potential (28) we list in Table I the residues of some of the poles for several values of  $E_{c.m.}$ . It is apparent there that the residues are large, if the poles are close to the imaginary axis. It is also seen, as we remarked above, that the cutoff-type singularities have comparatively small residues, but at least those associated with  $p_0$  cannot be ignored.

In order to investigate the behavior of  $S(\lambda)$ , off the pole positions in the complex plane, we calculated  $S(\lambda)$  along various paths in the  $\lambda$  plane shown

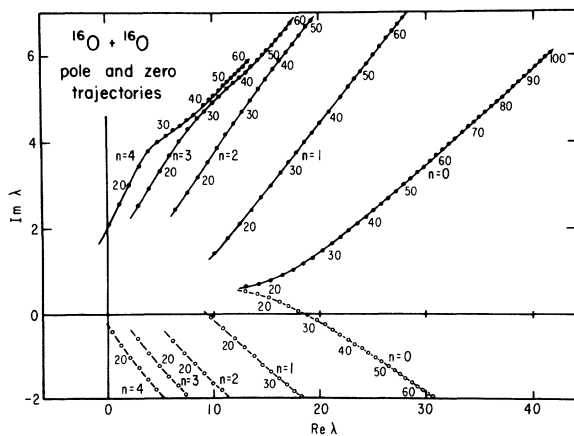


FIG. 4. Trajectories of poles (solid) and zeros (dashed) for the  $^{16}\text{O}$ - $^{16}\text{O}$  elastic scattering for the angular-momentum-independent potential (27). The notation is the same as in Fig. 3. Here the trajectories are traced up to 60 to 100 MeV to observe their asymptotic behavior in energy.

TABLE I. Residues  $|\beta_n|$  of the Regge poles for  $^{16}\text{O}$  elastic scattering for potential (28).  $p_0$  and  $p_{-1}$  give the summed residues of all poles associated with the cutoff singularities nearest to the real axis in the upper and the lower half plane.

Pole	$E_{c.m.}$ (MeV)		
	20	25	30
$n=0$	0.56	0.58	0.80
$n=1$	1.79	1.44	1.24
$n=2$	2.02	0.73	0.16
$n=3$	5.55	0.76	0.14
$n=4$	48.20	2.44	0.24
$p_0$	0.17	0.39	0.41
$p_{-1}$	0.02	0.06	0.09

in the upper left corner in Fig. 5. The value of  $|S(\lambda)|$  along these paths is shown in the same figure. As is seen the behavior for  $|\lambda| \rightarrow \infty$  follows what was predicted by Eqs. (11) and (12). Note, however, that along the positive imaginary axis,  $|S(\lambda)|$  first increases very fast to a very large value before it starts to decrease exponentially.

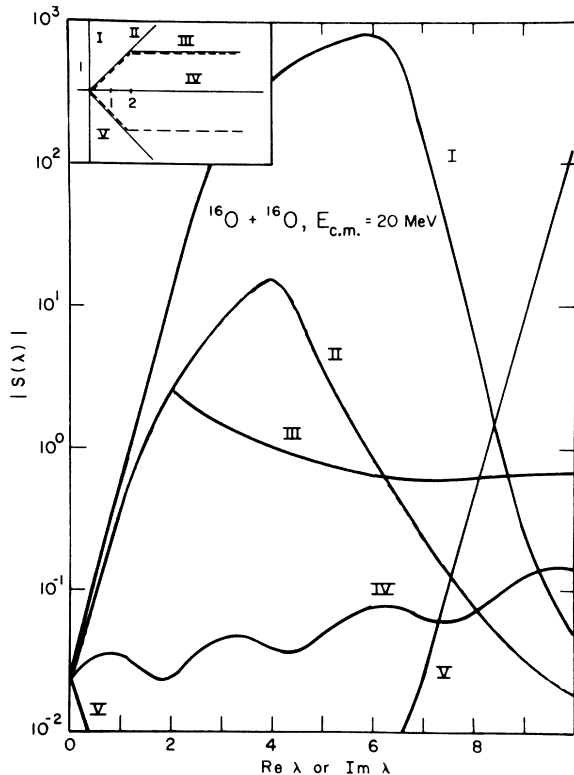


FIG. 5. Behavior of  $S(\lambda)$  in the right half plane for the  $^{16}\text{O}$ - $^{16}\text{O}$  elastic scattering for potential (28) at  $E_{c.m.} = 20$  MeV. The value of  $|S(\lambda)|$  is given along various paths described in the inset. The dashed line in the inset shows the path along which the background cross section given in Fig. 6 was calculated.

This will be seen to be related to the presence of pole trajectories with large residues close to the positive imaginary axis, as we remarked in relation to Table I.

In Fig. 6, we give the excitation function of the scattering cross section at  $90^\circ$  c.m. angle, and there the background term was calculated along the dashed line of Fig. 5, which encloses only the  $n=0$  SPR-type pole, as well as the  $p_0$  and  $p_{-1}$  cutoff singularities, as can be inferred from the behavior of the trajectories in Fig. 3.

The cross section for the sum of pole and background terms, i.e.,  $d\sigma^{(R,T)}$ , of course agrees with the exact calculation,  $d\sigma^{(B)}$ , which fits experiment rather well. The cross section  $d\sigma^{(R,B,n=0,p_0,p_{-1})}$  is seen to vary slowly with energy, having about the correct magnitude. On the other hand  $d\sigma^{(R,P,n=0,p_0,p_{-1})}$  is seen to be responsible for giving the correct oscillatory nature to the excitation function. The curve  $d\sigma^{(R,P,n=0-4)}$  was obtained by considering the five SPR-type poles of Fig. 3. As is seen, they give much too large cross sections at the lower energies. The reason is clearly the very large residues associated with the  $n=4$  trajectory (see Table I). Unless this large contribution is offset by similarly large background terms, calculated

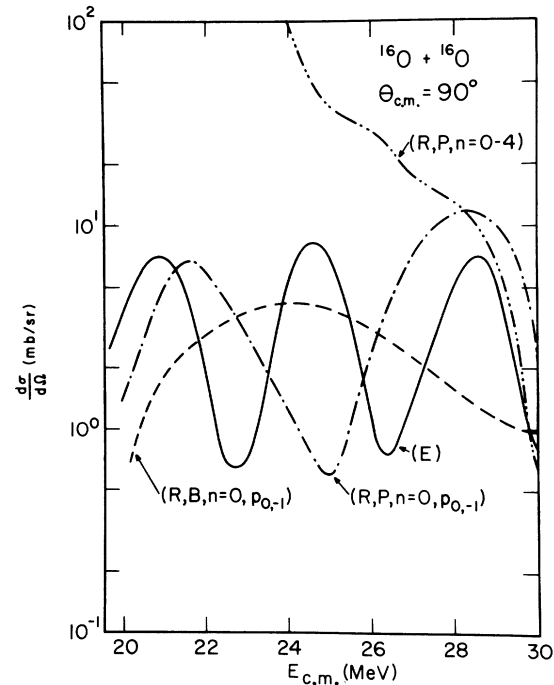


FIG. 6. Excitation function at  $90^\circ$  of the  $^{16}\text{O}$ - $^{16}\text{O}$  scattering cross section for the potential (28). Shown are the exact optical-model result and the cross sections in the Regge representation with the  $n=0$  pole term (including also the poles of the  $p_0$  and  $p_{-1}$  singularities), the  $n=0-4$  pole terms, and with the background term only.

anew along a path appropriately chosen, exact results cannot be reproduced. This result thus gives again a warning to a naive expectation that increasing the number of poles only can improve the accuracy of the calculations.

The "exact" cross section in Fig. 6 was of course obtained by symmetrizing the amplitude for the system of identical Bosons (this time two  $^{16}\text{O}$  nuclei), and including the Coulomb amplitude. In such a calculation, however, it is rather difficult to see clearly the relative importance of the pole and background terms, particularly when we are interested in the angular distribution. Even if the symmetrization is suppressed, the large Coulomb amplitude still somewhat obscures the situation. We thus calculated cross sections suppressing both Coulomb and symmetrization and the result obtained for  $E_{c.m.} = 20$  MeV is presented in Fig. 7. As is seen the magnitude and the oscillatory nature at forward angles is mostly due to the back-

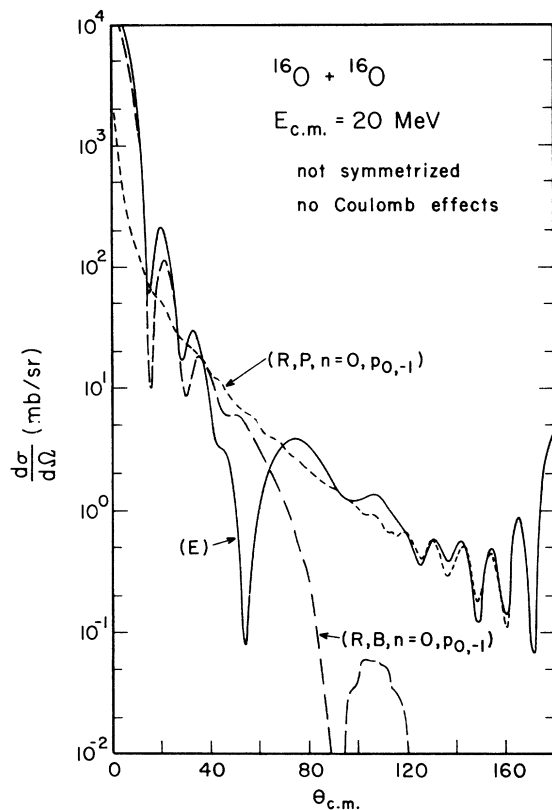


FIG. 7. Differential cross sections of the  $^{16}\text{O}$ - $^{16}\text{O}$  scattering for the potential (28). Here the cross section is calculated without symmetrization and by suppressing completely Coulomb effects (even though these were included in the  $S$ -matrix calculation), to show the relative contributions of the pole and the background term. Shown are the pole and the background cross sections in the Regge representation with the  $n=0$  pole (including also the poles of the two closest cutoff singularities).

ground term alone, although a very deep minimum at  $55^\circ$  is due to its destructive interference with the pole term. On the other hand, the magnitude as well as the oscillatory nature of the backward-angle cross section are almost entirely due to the pole term alone.

This general feature has already been noticed in Refs. 3 and 4, in fitting the  $\alpha$  and  $^{16}\text{O}$  scattering with the pole-plus-background model. If a Regge pole  $\lambda = \alpha_0 + \frac{1}{2}$  dominates the backward-angle cross section, the angular distribution there is approximately proportional to  $|P_{\alpha_0}(-\cos\theta)|^2$ , if there is no Coulomb interaction. The Coulomb interaction, however, does not change this angular distribution significantly, though it changes the magnitude by a factor  $|\exp(2i\sigma_{\alpha_0})|^2$ . Therefore, under some circumstances it is possible to determine the approximate position of the Regge pole by simply knowing the oscillatory nature of the experimental cross section at large angles.<sup>22</sup>

#### VI. COMPARISON WITH THE PARAMETRIZED $S$ MATRIX OF McVOY

McVoy<sup>4</sup> made a detailed study of the usefulness of a parametrization of the  $S$  matrix, with a one-pole-plus-background representation of the form given in (15), for the scattering of  $^{16}\text{O}$  by  $^{16}\text{O}$ . He did not attempt to fit the experimental cross sections, but rather exact theoretical cross sections obtained with the conventional optical-model calculations made with the optical potential (27), except that its imaginary part was replaced by

$$\begin{aligned} W &= (-17.2 + 1.86E_{c.m.}) \text{ MeV}, \\ R_l &= 4.17 \text{ fm}, \quad a_l = 0.805 \text{ fm}. \end{aligned} \quad (30)$$

As is seen in Fig. 6 of Ref. 4, McVoy's fit to the exact cross sections was quite good for  $E_{c.m.} \geq 24$  MeV, but became worse for lower  $E_{c.m.}$ . In particular, at  $E_{c.m.} = 20$  MeV no satisfactory fit was obtained.

By looking at Fig. 6 of Ref. 4 one may conclude, as did McVoy, that (15) works well when it is used to fit an angular distribution which has a smooth midsection. Comparing Fig. 6 with Fig. 7 both of Ref. 4, one may further say that the condition of getting such a smooth midsection is that the background part of the  $S$  matrix dominates in the forward angles, but falls off rather fast with increased angle. Then the magnitude and the oscillation at large angles can be accounted for entirely by the pole contribution, the oscillation in the smaller angles being due to the interference between the pole and background contributions. If the pole lies fairly close to the real axis of the

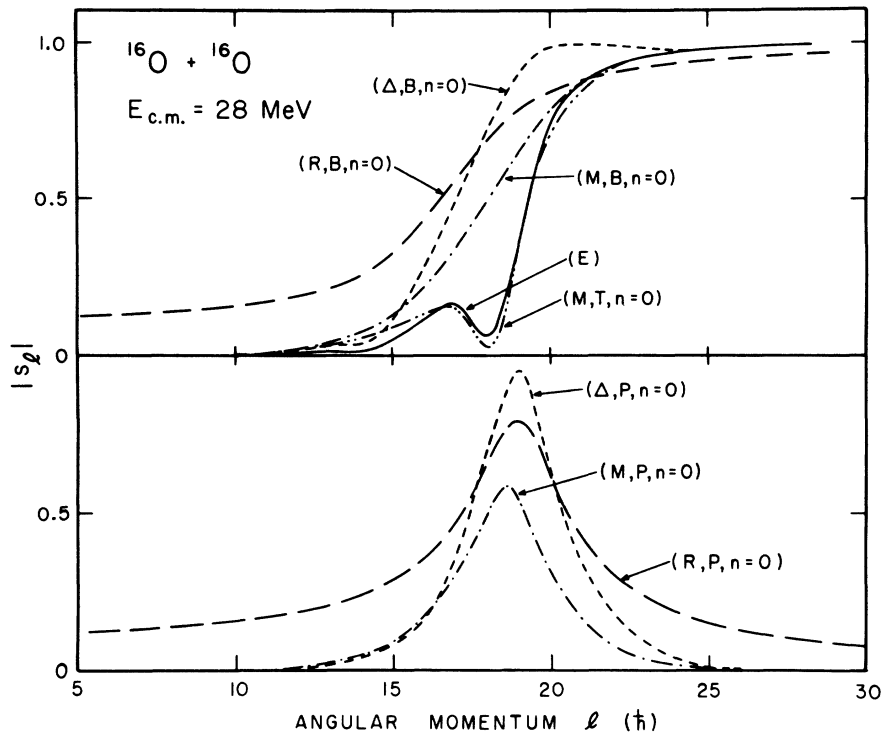


FIG. 8. Absolute value of the S matrix elements of the  $^{16}\text{O}$ - $^{16}\text{O}$  scattering for the potential (30) at  $E_{c.m.} = 28 \text{ MeV}$ , calculated in the Regge and  $\Delta$  representations and from the S-matrix parametrization (14). The upper half gives curves for total S matrix elements (T) and for those calculated from the background only (B), while the lower part gives those of the pole terms (P).

angular momentum plane, only one or two Legendre polynomials are involved in the pole term. Since these Legendre polynomials usually have high orders, their values in the midsection are small, accounting for the smooth midsection.

Having thus understood that the smooth midsection is due to the separate contributions of the pole and background terms in different angular regions, it would be instructive to look at the same thing in terms of the different behavior of the pole and background S matrix  $S_l$  as a function of  $l$ . The absolute values of  $S_l$  calculated at  $E_{c.m.} = 28 \text{ MeV}$  are presented in Fig. 8, in various representations. [For notations see the end of Sec. III. We also note that in calculating  $|S_l|$  the 1 on the left side of Eq. (7) was included into the background term on the right-hand side.] In general  $|S_l^{(B)}|$  for the background terms increases smoothly from zero for lower  $l$  to unity for higher  $l$ . The interval in  $l$ , in which  $|S_l^{(B)}|$  increases from 0.1 to 0.9, may somewhat vaguely be called the "active region" of  $S_l^{(B)}$ . If this region is narrow, we say that the "cutoff" is "steep."

As is seen in Fig. 8 the active region of  $S_l^{(M,B,n=0)}$ , the McVoy background term, is localized rather narrowly, and so is  $S_l^{(M,P,n=0)}$ . Compared with

these the corresponding curves for the Regge representation  $S_l^{(R,B,n=0)}$  and  $S_l^{(R,P,n=0)}$  are rather poorly localized. Since they are obtained exactly, there is nothing wrong in using them, but in assessing the validity of McVoy's parametrization, it is more convenient to use another representation, and for this purpose we introduced the  $\Delta$  representation, defined in Eq. (17). The  $|S_l^{(\Delta)}|$  curves are also presented in Fig. 8 and as is seen they now behave rather similar as  $|S_l^{(M)}|$ . (We use  $\Delta = 1.62$  as in McVoy's fit, but the results are not sensitive to the value of  $\Delta$  used.) For both, McVoy's parametrization and the  $\Delta$  representation, it is seen that  $|S_l^{(T)}| < |S_l^{(B)}|$ , i.e., the pole term interferes destructively with the background. It is further seen, that this interference causes the appearance of a dip in the  $|S_l^{(T)}|$  curve, its position being very close to the peak position of the pole term. Since it is known that at  $E_{c.m.} = 28 \text{ MeV}$  McVoy's approximation works well, we may say that when  $|S_l^{(B)}|$  has a comparatively narrow active region and a single dip is superposed upon it, (15) can be used to approximate it to a high accuracy. Anyway it would be worthwhile to emphasize here the very close similarity of behavior between  $|S_l^{(T,B)}|$  and  $|S_l^{(T,M)}|$  curves seen in Fig. 8.

The dip that appears in the  $|S_l^{(r)}|$  is naturally associated with the "zero" of  $|S_l^{(r)}|$ , and in this sense it is interesting to compare the behavior of pole and zero trajectories of the exact and approximate calculations. The results are given in Fig. 9, where, in calculating the trajectories of (15), the parameters given in Table I of Ref. 4 were used. As is seen in this figure the behavior of both ( $n=0$ ) pole and zero trajectories are very close to one another for  $E_{c.m.} \geq 24$  MeV, presenting another reason why (15) worked at higher energies. The trajectory behaves rather differently at lower energies, where (15) is known to fail.

Since we have obtained an idea of the behavior of  $|S_l|$  for the cases in which (15) works, we may now proceed to lower energies and see how  $|S_l|$  behaves differently, and the results obtained for  $E_{c.m.} = 18$  MeV are given in Fig. 10. The exact curve for this energy  $|S_l^{(B)}|$  shows two dips within its active region; those corresponding to the  $n=0$  and the  $n=1$  zeros. This causes the over-all cutoff of  $S_l$  to be steeper. McVoy's one-pole model fit  $|S_l^{(M,T,n=0)}|$  fails significantly in reproducing this behavior. The background attempts to reproduce the sharp, average slope of the cutoff, and this results in a too weak and misplaced pole. The  $n=0$  pole contribution in the  $\Delta$  representation  $|S_l^{(\Delta,P,n=0)}|$

is much stronger and produces the first dip in the  $|S_l^{(r)}|$  curve through destructive interference with the background.

Since the  $n=1$  zero is seen to be important in the  $S_l$  curves, it is interesting to investigate two-pole representations. McVoy also attempted this by extending his parametrization (15) to include two-pole zero factors;

$$S = B(l) \prod_{n=0}^N \frac{l - L_n - iz_n}{l - L_n - i p_n}, \quad (31)$$

where  $N=1$ . Also the residue parameter  $D_n = p_n - z_n$  was allowed to take complex values for  $n=0$ . The pole and zero positions for this fit are also shown in Fig. 9. Not only is the agreement with the exact positions worse for  $n=0$ , but also the imaginary parts for the  $n=1$  pole and zero are completely wrong. The  $|S_l|$  values for this fit and for the two-pole  $\Delta$  representation are also included in Fig. 10. The curve  $|S_l^{(M,T,n=0,1)}|$  shows even poorer agreement with the exact curve than that for the one-pole fit and the pole terms are still too weak. The corresponding background  $|S_l^{(\Delta,B,n=0,1)}|$  is smoother and less steep than that of the one-pole  $\Delta$  representation. Thus although McVoy's two-pole parametrization did give a bet-

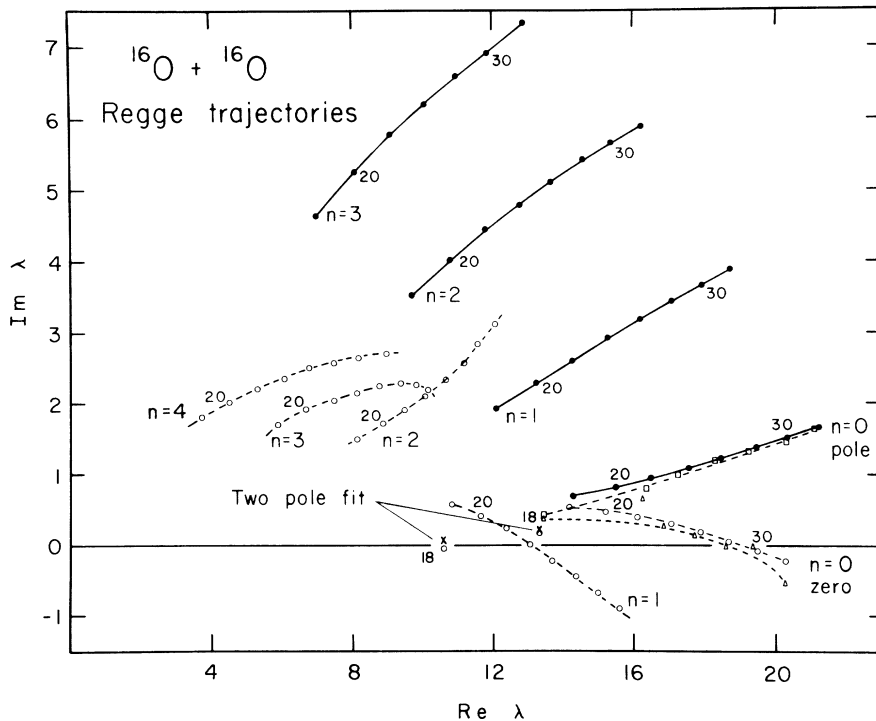


FIG. 9. Trajectories of poles (solid) and zeros (dashed) for the  $^{16}\text{O}-^{16}\text{O}$  scattering for the potential (30). Also shown are the trajectories for the  $n=0$  pole (squares) and zero (triangles) as determined from the  $S$ -matrix parametrization of McVoy. The  $n=0$  and 1 pole and zero positions at 18 MeV for the two-pole parametrization (31) are also indicated.

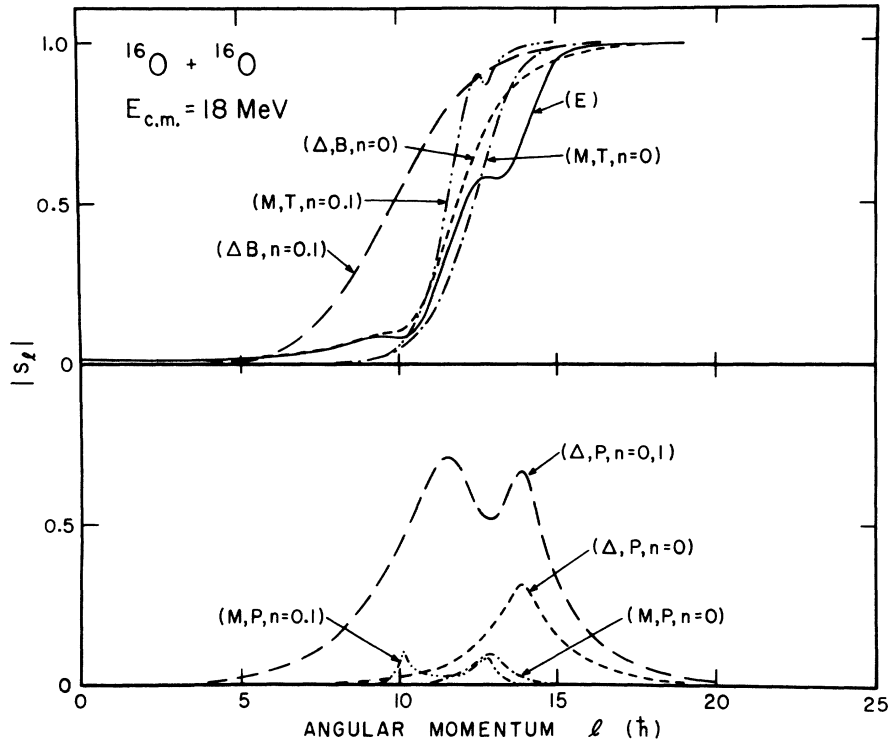


FIG. 10. Same as Fig. 8, except that the calculation was made here at  $E_{c.m.} = 18$  MeV, and that results with two poles are also included.

ter fit to the angular distributions (Fig. 10 of Ref. 4), this could have been only fortuitous. Since the cutoff of the background is so steep, it is very likely that the backward-angle oscillations in his fit arose from the background term alone, and that the poles did not contribute to the angular distribution in any significant way, contrary to what the exact calculation shows. These difficulties, however, do not mean that the two-pole model can never be useful. It may simply be a matter of a further search for parameters, and we give in Sec. VII a suggestion for an improved way of doing this.

After seeing the behavior of  $S_l$  we shall now discuss the angular distribution at  $E_{c.m.} = 18$  MeV, and thus give in Fig. 11 the one- and two-pole angular distributions for the  $\Delta$  representation together with the exact one. It is seen that  $d\sigma^{(\Delta, B, n=0)}$  falls off rapidly with angle and is fairly smooth also at backward angles. On the other hand  $d\sigma^{(\Delta, P, n=0)}$  contributes mainly at large angles and accounts completely for the backward rise and oscillation of the angular distributions. Note that  $d\sigma^{(\Delta, P, n=0)}$  mainly consists of the  $l=14$  partial wave, as is seen from the fact that it has 14 minima and large oscillations at backward and forward angles but not in the midsection.<sup>23</sup> Thus we find that the one-pole  $\Delta$  representation does provide even at this lower en-

ergy a clear separation of the roles of the pole and background terms in different regions of scattering angle, a situation which was the case only at higher energies, if McVoy's parametrization was made.

In the two-pole  $\Delta$  representation, the pole term  $d\sigma^{(\Delta, B, n=0, 1)}$  gets much larger and contributes to the angular distribution also at intermediate angles. The two-pole background  $d\sigma^{(\Delta, B, n=0, 1)}$  is now completely smooth except at extreme backward angles, showing that the residual oscillation in the one-pole background  $d\sigma^{(\Delta, B, n=0)}$  was due to the  $n=1$  pole. At backward angles the one- and two-pole representations coincide, indicating that this region is still dominated by the  $n=0$  pole. Because of the increased pole contribution, the relative contributions of the pole and background terms are less clearly separated in the two-pole  $\Delta$  representation, than they were in the one-pole  $\Delta$  representation. However, the fact that  $d\sigma^{(\Delta, B, n=0, 1)}$  is straight may be significant in the sense that it behaves as  $d\sigma^{(\Delta, B, n=0)}$  does at higher energies.

Coming back to our statement that the one-pole-plus-background parametrization works well if the cutoff is sufficiently steep so that only one pole lies within its active region, we shall now investigate a little further the physical situation under which such a favorable condition is realized.

It was already discussed in some detail in Ref. 4 why the one-pole parametrization improves with increasing energy. The reason is that generally the  $l$  value at which the cutoff takes place increases faster with energy than does the real part of the pole position. (Compare e.g. the position of the  $n=0$  dip relative to the cutoff in Figs. 8 and 10.) Therefore, as long as the cutoff is reasonably sharp, there will eventually be realized a situation in which only the  $n=0$  pole exists within the active region and then a one-pole parametrization is possible. An instructive experimental example of this effect can be found in the comparison of the  $\alpha$ -scattering data at 30 MeV<sup>3</sup> and 80 MeV,<sup>24</sup> where the latter shows the characteristic smooth midsection in the angular distribution. At still higher energies even the  $n=0$  pole cannot lie in the active region and then the cross section will be simply described by the background term only.

We expect that another factor which determines the applicability of a one-pole parametrization is the strength of the absorption, because this controls the steepness of the cutoff. To investigate this further we give in Fig. 12 the pole and zero positions as well as  $|S_l|$  calculated at  $E_{c.m.} = 16$  MeV with potential (27) except that  $W$  takes the values 1 and 5 MeV. It is seen that the effect of the increase of  $W$  on the poles and zeros is an almost

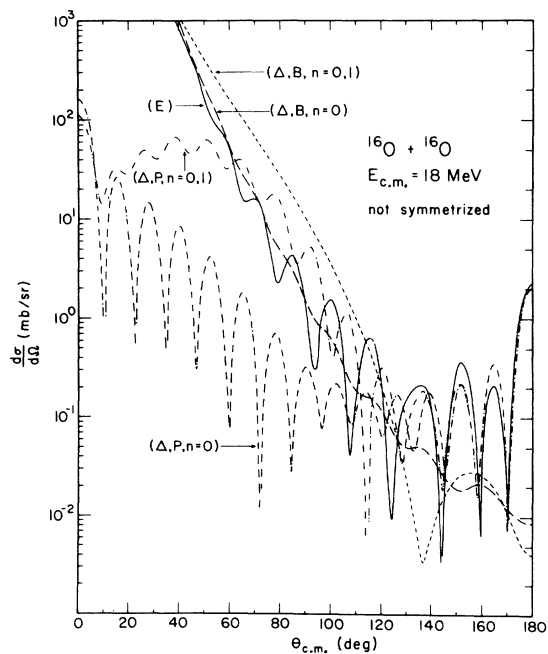


FIG. 11. Differential cross section of the  $^{16}\text{O}$ - $^{16}\text{O}$  scattering with the potential (30) calculated at  $E_{c.m.} = 18$  MeV. Shown are the exact cross section and those calculated in the  $\Delta$  representation for one- and two-pole terms and the corresponding background terms.

uniform shift of their positions in the direction of the positive imaginary axis. The  $|S_l^{(E)}|$  curve for  $W=1$  MeV has a rather marked structure whose dips are caused by the zeros of the  $S$  matrix. As  $W$  increases the dips become shallower, because the zeros move away from the real axis, and more importantly the magnitude of  $|S_l|$  on the average decreases for lower  $l$  values making the dips less important and the cutoff steeper. Thus the one-pole parametrization becomes better with increasing absorptive strength.

At this point it might be worthwhile to comment further on a statement made by McVoy with reference to his Fig. 4. There he displays  $|S_l^{(E)}|$  curves similar to those shown in our Fig. 12 (the potentials are very similar in the two cases) and argues that the overlapping contributions of different poles give rise to the smooth cutoff  $S$  matrix and that the smoothing with increasing absorption is due to an increasing overlapping of the resonances. To test this statement we show in Fig. 12 also  $|S_l^{(R, P, n=0-2)}|$ ,

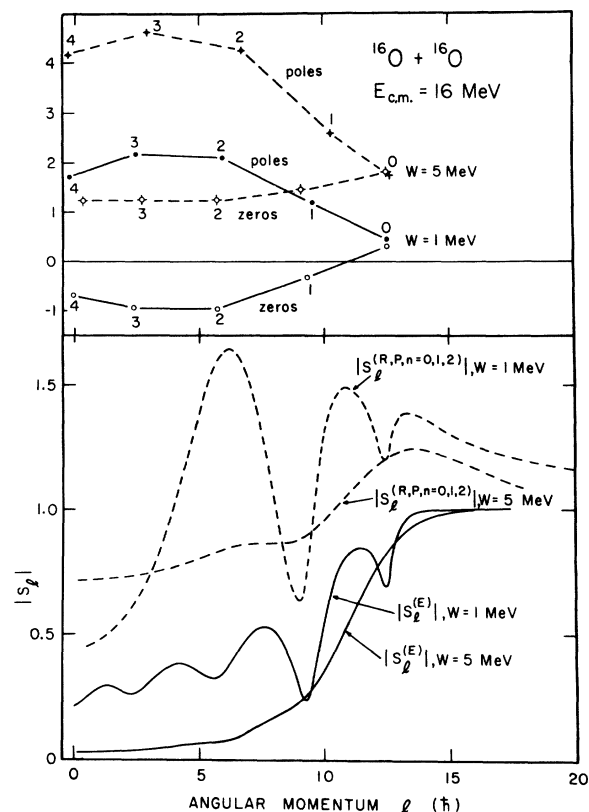


FIG. 12. The upper part shows pole and zero positions for the  $^{16}\text{O}$ - $^{16}\text{O}$  scattering with the potential (27) but with  $W=1$  and 5 MeV. Poles and zeros for each value of  $W$  are connected by lines to guide the eye. The lower part shows exact  $S$  matrix elements for these two values of  $W$  and those calculated from the Regge representation with the  $n=0-2$  pole terms only.

i.e., the  $S$  matrix resulting from the first three pole terms of a Regge representation.<sup>25</sup> Even though these curves have some similarity in shape with the exact one, particularly being smoother for stronger absorption, the magnitude of  $|S_l|$  is much too large for the lower  $l$  values. Therefore the overlap of a few poles alone cannot produce the smooth and sharp cutoff. The background term contributes significantly at the same time.

In order to discuss finally the interplay between the values of  $W$  and  $E_{c.m.}$ , we shall discuss here a remark made by McVoy<sup>4</sup> that he used potential (30), instead of (27), because the latter had several active poles, which prevented him from using the one-pole parametrization. This statement seems rather surprising at first, if one notices that at least the  $n=0$  and  $n=1$  pole positions for the potential (27) (seen in Fig. 4) are very close to those of the potential (30) (seen in Fig. 8), and further that their residues are about the same. It should be noted, however, that the behavior of the zeros are quite different in these two potentials. In potential (27) all the zeros are close to the real axis at lower energies and consequently there are several dips in the  $|S_l|$  curve making the latter unsuitable for treatment with the one-pole parametrization. At higher energies, however, most of these zeros move away from the real axis and only the  $n=0$  zero remains important. In fact the angular distribution for the potential (27) calculated, e.g. at  $E_{c.m.}=32$  MeV has a smooth midsection, showing that McVoy's parametrization could have been used. The potential (30), on the other hand, has a much stronger absorption (though only at a shorter distance in the coordinate space), and this pushes up the poles and zeros in the lower  $l$  region away from the real axis. This makes the cutoff steeper and thus allows one to use the one-pole parametrization even at lower energies. This way it is clear that the energy and the strength of absorption combined decide whether the one-pole parametrization is possible or not.

## VII. CONCLUSIONS AND DISCUSSIONS

We investigated in considerable detail the analytic properties, in the complex angular momentum plane, of the  $S$  matrix of conventional optical models of the Woods-Saxon form. It was shown that they are quite different from those of Yukawa potential, on which many of the previous arguments of the Regge technique had been based.<sup>6, 10</sup> One important change is that the trajectories are almost straight and never seem to turn back into the left half plane with increased energy. Moreover, there are additional poles, if a potential with an angular momentum cutoff of the imaginary

part is used. At the same time the behavior of the  $S$  matrix is such that the background integral can never be taken along the imaginary axis, but has to be bent eventually to run parallel to the real axis. This fact seems to indicate that one should use a representation in which the background integral is retained explicitly, in one way or another. In other words an attempt to replace accurately the whole amplitude in terms of pole terms alone seems very difficult to achieve in general.

Considerably detailed arguments were also made in assessing the validity of the one-pole-plus-background parametrization. As was stated towards the end of Sec. VI, we believe that this approach does work, if the energy under consideration is sufficiently high, and if the system treated is strongly absorptive. Many present experimental results for heavy-ion scattering, however, do not seem to realize such favorable circumstances. Thus the smooth midsection in the differential cross section, which is characteristic of a process dominated by only one Regge pole, is more the exception than the rule. E.g. in  $\alpha$  scattering one has to go as high as 80 MeV for this phenomenon to be realized. In this respect it should be interesting to investigate more closely scattering between nonidentical particles where the behavior of the angular distribution at backward angles is not obscured.

It is thus seen that in order to be able to fit, with Regge technique, the large amount of existing and forthcoming data, it is desirable to have a knowledge of how to extend the one-pole-plus-background parametrization. One answer to this question may be to use Eq. (31), i.e., the two-pole- (or more-pole) plus-background parametrization. McVoy<sup>4</sup> already used this, but without much success, perhaps because he did not have a guiding principle to limit the possible region of the parameters.

From the results given in Figs. 3 and 9, however, it seems that such a two-pole parametrization of a heavy-ion reaction should have the following features. The cutoff should be less steep than in the one-pole case to accommodate several poles, and possibly it should also be modified to allow for less absorption of the lower partial waves. The  $n=0$  and  $n=1$  poles are spaced at least two units of angular momentum apart, and only for  $n=0$  are the pole and zero positions close together, while for  $n>0$  the pole but not necessarily the zero position is usually removed from the real axis by at least one unit. The phase between the pole and background terms should be such that they interfere destructively, because  $|S_l^{(E)}| < |S_l^{(B)}|$  as is seen in Figs. 8 and 10. These conclusions are only based on the examples considered so far in this work and they may prove to be not universal

enough. Nevertheless, tests of these principles are underway and results will be reported shortly.

So far we have restricted our arguments entirely to elastic scattering. The method can be extended without very much modification to transfer reactions, if it is desired. This is seen by writing the distorted-wave Born approximation in the source term formalism.<sup>26</sup> In that case the outgoing particle is described by an inhomogeneous equation, the inhomogeneity giving the source of the ampli-

tude due to the incident channel. Such an equation is not more difficult to handle numerically than the corresponding homogeneous equation. Also the analytic behavior of the source term in the complex plane should be fairly transparent.

We are indebted to a very useful conversation with Professor K. W. McVoy. Careful reading of the manuscript by W. R. Coker is cordially acknowledged.

---

\*Work supported by Heinrich-Hertz-Stiftung des Landes Nordrhein-Westfalen, Germany.

†Work supported in part by the U. S. Atomic Energy Commission under Contract No. AT-(40-1)-2972.

<sup>1</sup>T. Regge, *Nuovo Cimento* **14**, 951 (1959); **18**, 947 (1960); A. Bottino, A. M. Longoni, and T. Regge, *ibid.* **23**, 954 (1962).

<sup>2</sup>T. E. O. Ericson, in *Preludes in Theoretical Physics*, edited by A. de-Shalit *et al.* (North-Holland, Amsterdam, 1965).

<sup>3</sup>A. A. Cowley and G. Heymann, *Nucl. Phys.* **A146**, 465 (1970).

<sup>4</sup>K. W. McVoy, *Phys. Rev. C* **3**, 1104 (1971).

<sup>5</sup>E. A. Remler, *Phys. Rev. A* **3**, 1949 (1971).

<sup>6</sup>S. Mukherjee, *Phys. Rev.* **160**, 1546 (1967).

<sup>7</sup>S. Mukherjee and C. S. Shastri, *Phys. Rev.* **169**, 1234 (1968).

<sup>8</sup>S. Mukherjee and C. S. Shastri, *Nucl. Phys.* **A128**, 256 (1969).

<sup>9</sup>R. Shanta and C. S. Shastri, *Phys. Rev.* **176**, 1254 (1968); R. Shanta and R. K. Satpathy, *Phys. Rev. C* **2**, 1279 (1970).

<sup>10</sup>R. G. Newton, *The Complex  $j$ -Plane* (Benjamin, New York, 1964).

<sup>11</sup>T. Tamura and H. H. Wolter, *Bull. Am. Phys. Soc.* **16**, 624 (1971); **17**, 590 (1972).

<sup>12</sup>J. S. Blair, in *Lectures in Theoretical Physics*, edited by P. D. Kunz and W. E. Brittin (Univ. of Colorado Press, Boulder, Colorado, 1966).

<sup>13</sup>P. G. Burke and C. Tate, *Comput. Phys. Commun.* **1**, 97 (1969).

<sup>14</sup>F. Rybicki and T. Tamura, *Comput. Phys. Commun.* **1**, 25 (1969).

<sup>15</sup>E. S. Cambell *et al.*, MIT Technical Report No. 73, 1960 (unpublished).

<sup>16</sup>J. V. Maher, M. W. Sachs, R. H. Siemssen, A. Weidinger, and D. A. Bromley, *Phys. Rev.* **180**, 1665 (1969).

<sup>17</sup>R. A. Chatwin, J. S. Eck, D. Robson, and A. Richter, *Phys. Rev. C* **1**, 795 (1970).

<sup>18</sup>K. S. Low and T. Tamura, *Phys. Letters* **40B**, 32 (1972).

<sup>19</sup>A. Arima, G. Scharff-Goldhaber, and K. W. McVoy, *Phys. Letters* **40B**, 7 (1972).

<sup>20</sup>The positions of the poles as reported in Ref. 19 are different from ours by a few units of angular momentum. Although the poles are determined for a different potential in Ref. 19, it is doubtful whether the method for this determination was sufficiently accurate.

<sup>21</sup>It might be of interest to note, that for the  $l$ -dependent potential (28) the proportionality between  $l(l+1)$  and  $E_{c.m.}$  is almost as good as for potential (27), except for some slight irregularities, which result from the fact, that the energy dependence of  $l_c$  is not completely smooth, cf. Ref. 17. It was, moreover, stated in Ref. 19, that the  $l$ -dependent potential (28) does not exhibit resonance effects at all, for a reason we do not understand. Note that the behavior of the pole trajectories and the  $S$  matrix elements is very similar here as it was for the potential (27). Also in Fig. 7 there is clearly an indication of the  $n=0$  resonance in the angular distribution.

<sup>22</sup>J. T. Londergan and K. W. McVoy, *Bull. Am. Phys. Soc.* **17**, 590 (1972).

<sup>23</sup>This is in contrast to McVoy's pole angular distributions, which are smooth at forward angles. The source of this difference is that, in calculating these cross sections, he seems to have set  $B(\lambda)=1$ , leaving the pole term with substantial contributions from the lower partial waves. This is similar when the Regge representation is used, for which the pole term also falls off slowly for the lower partial waves, and for which the pole cross section is also smooth at forward angles, as is seen in Fig. 7.

<sup>24</sup>P. P. Singh, R. E. Malmin, M. High, and D. W. Devins, *Phys. Rev. Letters* **23**, 1124 (1969).

<sup>25</sup>If also the  $n=3$  and  $n=4$  poles are included, the  $S$  matrix elements generated become still larger, because these poles have very large residues, similar as those of potential (28) listed in Table I.

<sup>26</sup>R. J. Ascutto and N. K. Glendenning, *Phys. Rev.* **181**, 1396 (1969).